



1 Atmospheric Mixed Rossby Gravity Waves over Tropical Pacific 2 during the Austral Summer

3 Hugo A. Braga¹ and Victor Magaña¹

4 ¹Departamento de Geografía Física, Instituto de Geografía, Universidad Nacional Autónoma de México, 04510, México City,
5 México.

6 *Correspondence to:* Hugo A. Braga (hugoalvesbraga@icloud.com)

7 **Abstract.** Atmospheric Mixed Rossby-Gravity Wave (MRGW) activity during the austral summer months (Dec-Jan-Feb) is
8 examined by means of observational analyses for the 1991 - 2020 period. The main objective of the study is to explore the
9 relationship between tropical circulations at upper and lower tropospheric levels and tropical convective activity. Using an
10 Empirical Orthogonal Function (EOF) analysis of the high-frequency meridional component anomalies of the wind at 200 hPa,
11 for zonal wavenumber 5-6, episodes of intense MRGW activity are detected. Composite analyses based on an EOF analysis
12 show a quadrature phase over the central-eastern equatorial Pacific between the MRGW structure in the upper and lower
13 troposphere. Lagged correlations between the first two EOFs principal components, and the wind field and OLR, show that
14 MRGWs are laterally forced at upper tropospheric levels over the westerly duct region and later propagate westward and
15 downward. Once the MRGW reaches the lower tropospheric levels, it induces zones of moisture convergence that modulates
16 convective activity. Tropical convection develops in the divergent region of the MRGW at 200 hPa and in the MRGW moisture
17 convergence region at 700 hPa. Since the MRGW phase tilts eastward with height, moisture convergence at lower tropospheric
18 levels tends to coincide with divergence at upper levels favoring intense convective activity which results in the antisymmetric
19 outgoing longwave radiation anomalies off the equator near the MRGW. Therefore, the occurrence of MRGWs over the eastern
20 Pacific, is a form of tropical – extratropical interaction that generates tropical convection anomalies by means of induced lower
21 tropospheric moisture convergence and divergence anomalies.

22 **Keywords:** Mixed Rossby-Gravity Waves, Tropical–Extratropical Interactions, Lateral Forcing, Moisture Convergence.

23 1 Introduction

24 Equatorial waves are important elements of the atmospheric tropical circulations. Matsuno (1966) determined the main spatial
25 and temporal characteristics of Mixed Rossby-Gravity Waves (MRGWs), later identified by means of observational analyses
26 by Yanai and Maruyama (1966) and Maruyama (1967). MRGWs exhibit fluctuations in the meridional component of the wind,
27 with periods between 4 to 5 days and zonal wave numbers 4 to 6 (Yanai and Hayashi 1969; Yanai and Murakami 1970a, b;



28 Nitta 1970). Their vertical wavelengths range between 6 to 10 km (Holton 1979, Magaña and Yanai 1995) with an upward
29 propagation from the upper troposphere to lower stratospheric levels (Yanai and Hayashi, 1969).

30 The origin of MRGWs has been explored in several observational and model studies. Lateral forcing of MRGWs was originally
31 proposed in model studies by Mak (1969) and later explored by Bennet and Young (1971), Hayashi and Golder (1978) and
32 Zhang and Webster (1992), among others. Observationally, Yanai and Lu (1983), Magaña and Yanai (1995), Kiladis et al
33 (2009), Shreya and Suhas (2024) documented MGWs triggered by lateral forcing. On the other hand, tropical convective
34 heating has also been suggested as a mechanism that results in MRGWs (Holton, 1972; Hess et al., 1993). Hayashi (1970)
35 proposed that MRGWs could be the result of Wave-CISK, i.e., by means of the interaction between convective heating and
36 the wave itself. However, Takayabu and Nitta (1993) ruled out Wave-CISK as a mechanism to maintain MRGWs. Some of
37 these analyses also explore the role of MRGWs in modulating tropical convective activity (e.g., Magaña and Yanai 1995,
38 Kiladis et al 2009), but a definite answer to this problem has not been given.

39 The first observational studies on the vertical structure of MRGWs indicate that they extend from the troposphere to the lower
40 stratosphere (Yanai and Hayashi, 1969). A vertical node of these equatorial waves appears in the upper-tropospheric level
41 (around 200 hPa), and the phase tilts westward to lower tropospheric levels and eastward into the stratosphere (Magaña and
42 Yanai 1995; Zhou and Wang 2007; Kiladis et al., 2009). The tilting in MRGWs plays a crucial role in the vertical transport of
43 momentum and energy (Holton, 1979), but it may also be important in the spatial distribution of the convective activity
44 anomalies associated with MRGWs (Kiladis et al., 2009).

45 Recently, Shreya and Suhas (2024) confirmed that MRGWs are excited by lateral forcing from midlatitude disturbances from
46 the winter hemisphere. The propagation of these midlatitude waves into the tropics takes place across the eastern Pacific
47 westerly duct (Webster and Holton, 1982), which tends to remain “open” in the upper troposphere during the austral summer
48 months (Dec-Jan-Feb) (Braga et al., 2022). During the austral winter (Jun-Jul-Aug) the westerly duct periodically appears as
49 the Madden Julian Oscillation propagates along the eastern tropical Pacific, which allows the existence of MRGWs (Magaña
50 and Yanai, 1991). Therefore, lateral forcing as an excitation mechanism of MRGWs, takes place at upper tropospheric levels.
51 Eventually, MRGWs at higher tropospheric levels show in lower atmospheric levels, mainly towards the western Pacific region
52 (Au-Yeung and Tam 2018).

53 The processes involved in the downward phase propagation of a MRGW from upper to lower tropospheric levels, the near
54 boundary layer may modulate deep tropical convection. A study by Zhou and Wang (2007) shows that an upper tropospheric
55 MRGW acts as the precursor to a western Pacific tropical depression. Consequently, the downward phase propagation and the
56 vertical structure of the MRGW should be considered in the development of a region of intense convective activity around the
57 equatorial wave. These analyses suggest that as a MRGW, triggered at upper tropospheric levels propagates to lower
58 tropospheric levels, it may reflect in the modulation of moisture convergence and divergence near the boundary layer, that
59 ultimately controls deep convective activity in the equatorial regions.

60 As the westerly duct reaches maximum longitudinal extent and intensity, it allows the interhemispheric propagation of mid
61 latitude (Tomas and Webster, 1994; Li et al., 2015; Li et al., 2019; Braga et al., 2022) waves that are responsible for the



62 triggering of MRGW. Consequently, the existence of MRGWs and the corresponding antisymmetric anomalies in convective
63 activity (Kiladis et al 2009) may be considered part of a tropical-extratropical interaction process.
64 The present study aims at examining the characteristics and evolution of MRGWs, in the Pacific region, and the relationship
65 between this type of equatorial wave and convective activity off the equator, which remains as an open scientific question.
66 This study is structured as follows: Section 2 outlines the characteristics of the data used for the study and the methodology of
67 investigation. In Section 3, observational analyses are developed to determine the characteristics and evolution of MRGWs
68 and their relationship with convective activity. In Section 4 summary and conclusions are presented.

69 **2 Data**

70 **2.1 Data sets**

71 For the identification of MRGWs, global reanalyses of daily tropospheric winds and specific humidity ERA-5 for the period
72 1991 to 2020 (Hersbach et al., 2020) have been used. The spatial resolution of ERA-5 wind data is $2.5^\circ \times 2.5^\circ$ from 1000 to
73 100 hPa. Daily Outgoing Longwave Radiation (OLR) data from the National Oceanic and Atmospheric Administration
74 (NOAA) for the same period were also used (Liebmann and Smith, 1996) to document tropical convective activity anomalies.

75 **2.2 Vertically Integrated Moisture Flux**

76 The vertically integrated moisture flux field and its divergence were calculated to evaluate how atmospheric moisture is
77 distributed by tropical disturbances in the tropical regions. The VIMF is a measure of the amount of water vapor transported
78 in the atmosphere. Its convergence is used in the evaluation of the hydrological processes in the atmosphere (Fasullo and
79 Webster, 2003). High VIMF convergence (VIMFc) zones are related to intense convective activity. The VIMF has been used
80 to examine moisture transport processes, for instance in Easterly Waves (Pazos et al., 2023). The VIMF is calculated using the
81 expression:

$$82 \quad \text{VIMF} = \frac{1}{g} = \int_{p=1000}^{p=100} Vqdp \quad (1)$$

83 where q is the specific humidity ($\text{kg}\cdot\text{kg}^{-1}$), V is the horizontal wind field, g is the gravity constant, and p is the pressure
84 between 1000 and 100 hPa. VIMF units are $\text{kg}\cdot\text{m}^{-1}\cdot\text{s}^{-1}$.

85 **2.3 Methodology**

86 Various approaches have been used to diagnose MRGWs activity including spectral analysis with radiosonde data (Yanai and
87 Hayashi, 1969), using reanalysis data (Yanai and Lu, 1983; Magaña and Yanai 1995; Wheeler and Kiladis, 1999), or by
88 projecting meteorological wind fields of reanalysis data onto theoretical spatial structures of equatorial waves (Yang et al.,
89 2003; Au-Yeung and Tam, 2018). MRGWs patterns may be identified by means of Empirical Orthogonal Function (EOF)
90 analysis of the meridional component of the 200 hPa wind field. The Principal Components (PC1, PC2) of EOFs are used as

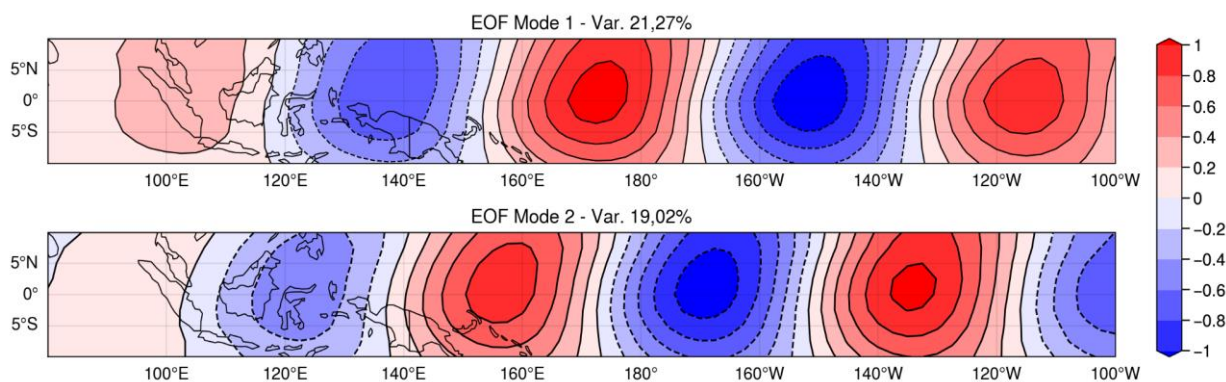


91 indices to compose wind, OLR, and atmospheric moisture fields to obtain the spatial characteristics of the MRGWs. The
92 identification of periods and regions of MRGW activity are determined based on the time series of intense signals in PC1 and
93 PC2. The temporal evolution of MRGW is examined by means of lagged – correlations of PC1 or PC2 and the wind, OLR and
94 moisture fields. For the present analyses, data are band-pass filtered with a Lanczos Filter (Duchon, 1979), in the period range
95 between 2 and 6 days. The spatial structure of the MRGW in the EOF analysis is captured with a spatial filter for zonal
96 wavenumbers 5 to 6 (Hayashi, 1982).

97 3. Results and Discussions

98 3.1 MGW Detection

99 The first EOF of the band-pass filtered component of the meridional wind (v) at 200 hPa, spatially filtered in the 5 and 6 zonal
100 wavenumber range, in the 10°N - 10°S, 80°E - 100°W domain shows the signal of a MRGW with a dominant zonal
101 wavenumber 5 (Fig 1). EOF2 also captures the MRGW signal but it is in quadrature with EOF1 which reflects the tendency
102 for the westward propagation of the wave. EOF1 explains 21.3% of the total variance, while EOF2 explains 19%.



103

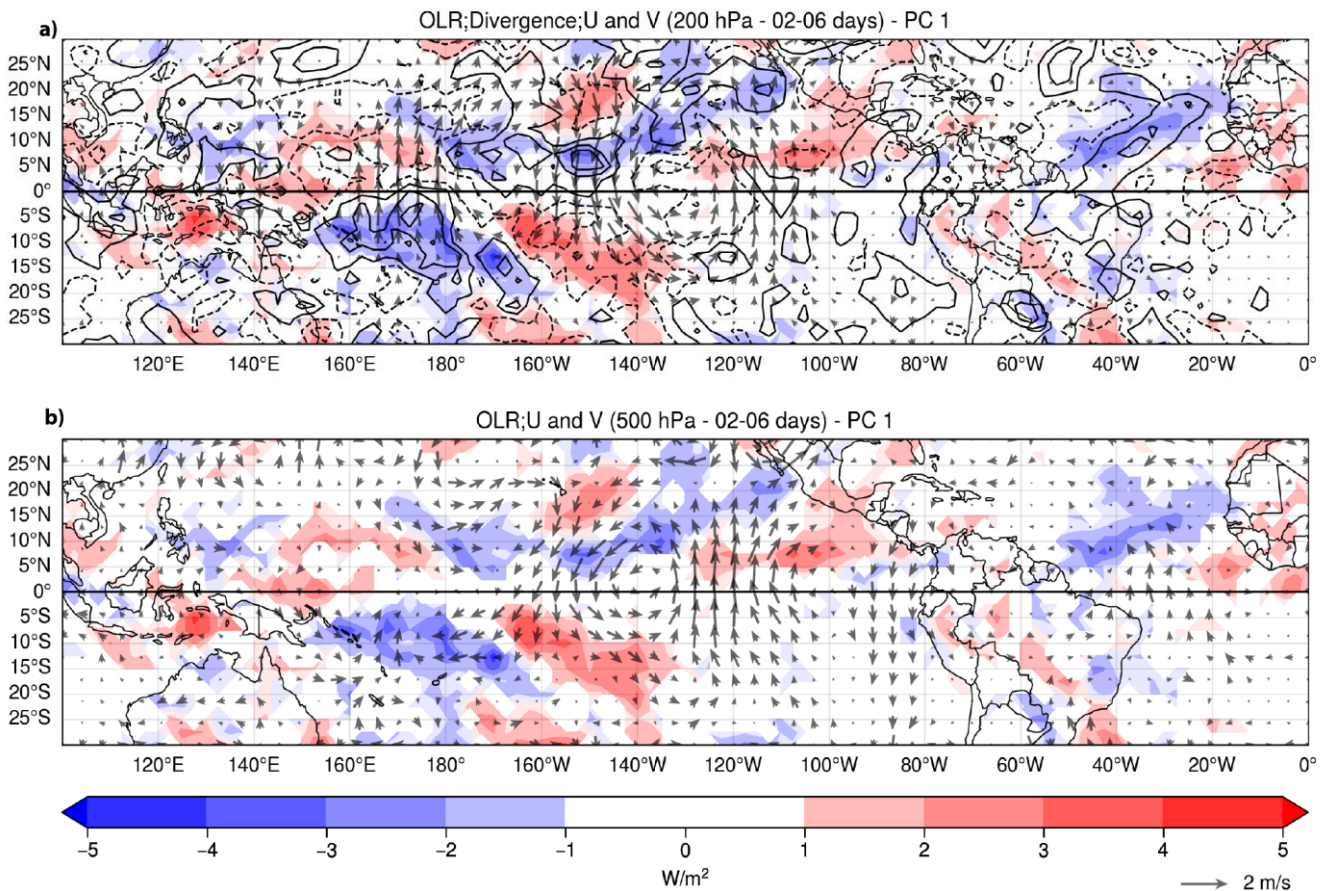
104 **Figure 1: First and second EOF for the 200 hPa space-time filtered anomaly of the meridional component of the wind field at 200**
105 **hPa for the December to February for the 1991 to 2020 period.**

106 To obtain the complete spatial structure of the wind field corresponding to a MRGW, composite patterns of the space-time
107 band-pass filtered wind fields at 200, 500 and 700 hPa were constructed using PC1 values above 1.0. The composite of the
108 wind field was combined with OLR anomalies at upper-levels and specific humidity anomalies at lower levels to obtain the
109 regions of the induced topical convective activity (Fig.2). Over the central eastern Pacific, a clockwise and an anticlockwise
110 circulation, centred along the equator show the expected anomalous wind field for a MRGW (Fig.2.a). In agreement with the
111 theoretical model of a MRGW, the convergent and divergent regions are anti-symmetrically located off the equator, between
112 the clockwise and anticlockwise circulations. The OLR anomalies associated with the MRGW coincide with the region of
113 convergence and divergence at upper tropospheric levels. At 500 hPa, the MRGW over the central Pacific is almost in phase
114 with its 200 hPa counterpart (Fig.2.b). When the signal of the MRGW is calculated at lower tropospheric levels it is observed
115 there is a phase shift towards the west in the clockwise and anticlockwise circulations. At 700 hPa, the intensity of the

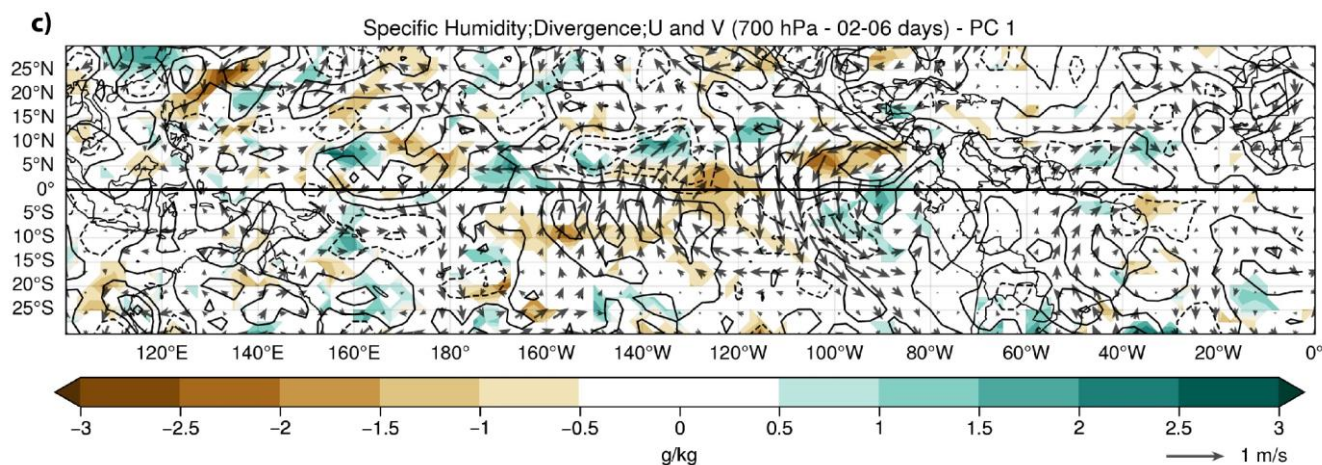


116 circulations is weaker than at upper tropospheric levels, but the regions of atmospheric moisture convergence and divergence
117 are observed off the equator in between the cyclonic and anticyclonic circulations. Just above the tropical boundary layer, the
118 zone of moisture convergence (divergence) is located at 140°W and 5°N to 10°N (5°S to 10°S) and at around 100°W and 5°S
119 to 10°S (5°N to 10°N), on the west and east sides of the clockwise circulation in the central Pacific (Fig.2.c). Moisture
120 convergence-divergence leads to increases-decreases of atmospheric humidity that tend to coincide with the regions of
121 negative-positive OLR anomalies. Such connections between upper and lower tropospheric levels around the MRGW
122 circulation suggest that tropical convection anomalies are generated at lower tropospheric levels through moisture
123 convergence, that coincide with regions of divergence and convergence at upper tropospheric levels due to the quadrature in
124 the MRGW between these two tropospheric levels.

125



126



127

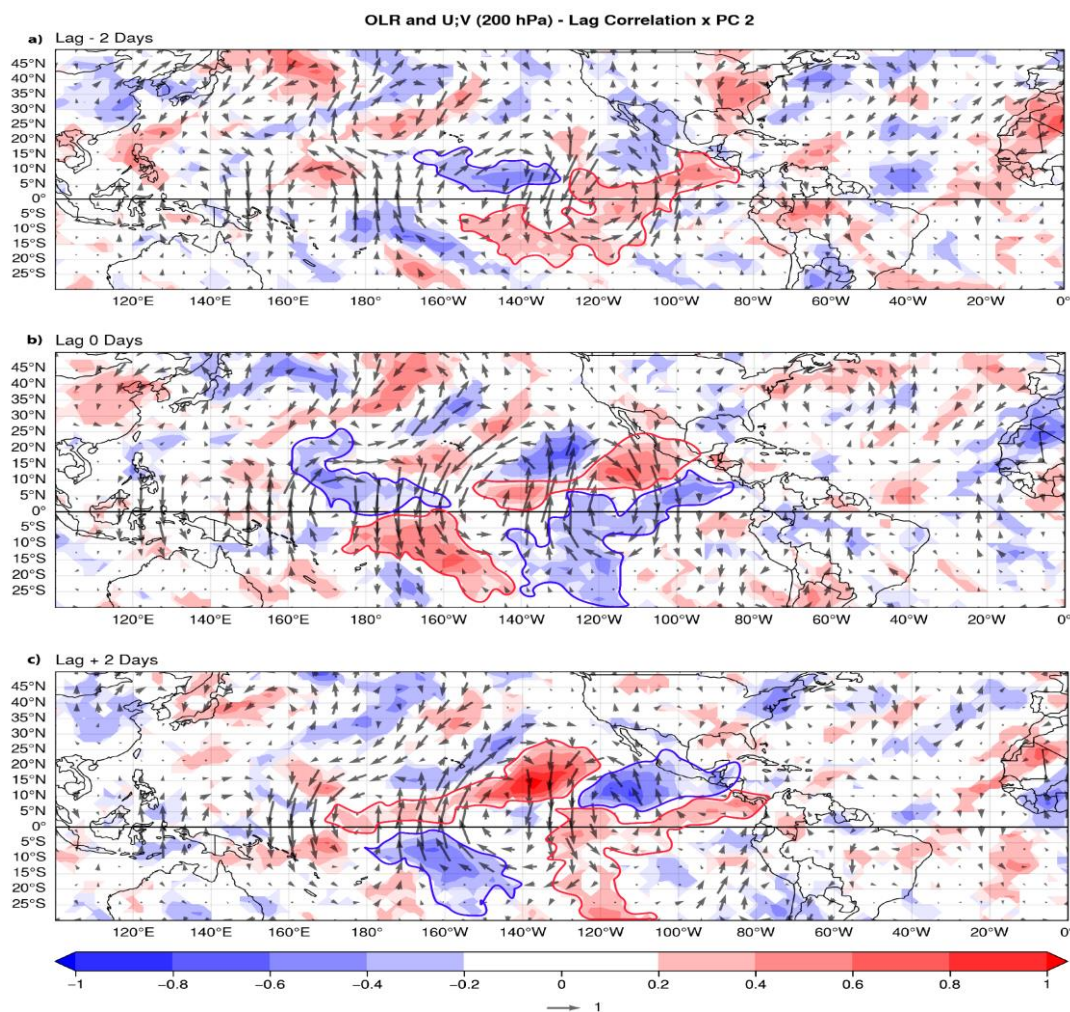
128 **Figure 2: Composite patterns based on PC1 > 1 conditions, showing band-pass filtered wind anomalies (2–6 day periods) at (a) 200**
129 **hPa, (b) 500 hPa and (c) 700 hPa. Wind anomalies are depicted as vectors, with dashed lines indicating convergence and solid lines**
130 **showing divergence. Shading represents outgoing longwave radiation (OLR) anomalies (red and blue) and specific humidity**
131 **anomalies (brown and green).**

132 As in previous analyses of the vertical structure of the MRGWs (Yanai and Hayashi, 1969; Zhou and Wang, 2007), the phase
133 of the wave tilts eastward with height, from 700 hPa to 200 hPa, in the troposphere, while the phases tend to tilt westward
134 from the upper troposphere to the lower stratosphere (Holton, 1979) reflecting the vertical structure of these equatorial waves.
135 As MRGW evolves across the Pacific, the zones of convergence and divergence move westward along with the corresponding
136 convective activity anomalies. The temporal evolution of a MRWG wind field and the associated tropical convection anomalies
137 may be analyzed by examining the sequence of events, from the onset of the equatorial wave around 200 hPa, to a few days
138 ahead, when its signal is observed at lower tropospheric levels. One point lagged correlations between PC2 and anomalies of
139 200 hPa wind and OLR in the -2 days to +2 days range show the evolution of a MRGW with an approximate 4 to 5 days
140 period. At lag -2 days, the correlation with the wind field shows the MRGW pattern over the central eastern Pacific with
141 vortices between 20°N and 20°S. In the central eastern an anticyclonic equatorial circulation is connected to a midlatitude wave
142 that emanates from the northwest Pacific (Fig. 3a). The cyclonic of this midlatitude circulation mechanically couples with the
143 MRGW that extends across the Pacific in a similar manner as the laterally forced MRGWs presented by Magaña and Yanai
144 (1995); Kiladis et al. (2009) and Shreya and Suhas, (2024). Over the central Pacific, negative (positive) OLR correlations
145 (anomalies) are observed between the clockwise and anticlockwise circulations of the MRGW over the equatorial region. The
146 OLR anomalies are modulated by the midlatitude wave train, following the ascending and descending motions described by
147 the omega equation. At lag 0 days, the MRWG propagates westward along with the antisymmetric anomalies in OLR around
148 the dateline (Fig.3.b), with a westward phase velocity of approximately 10 m·s⁻¹ and a zonal wavenumber 5. The modulation
149 of OLR anomalies by the midlatitude wave that propagates across the eastern tropical appears to extend to the Southern
150 Hemisphere to the western coast of South America, as previous analyses have shown (e.g., Braga et al 2022). At lag+2 days,
151 the regions of convergence and divergence off the equator, around 15-20° in latitude, displace westward along with the tropical



152 convection anomalies (Fig. 3c). At this stage the midlatitude wave train weakens but the MRGW remains and is clearly
153 observed over the westerly duct region and the western Pacific.

154

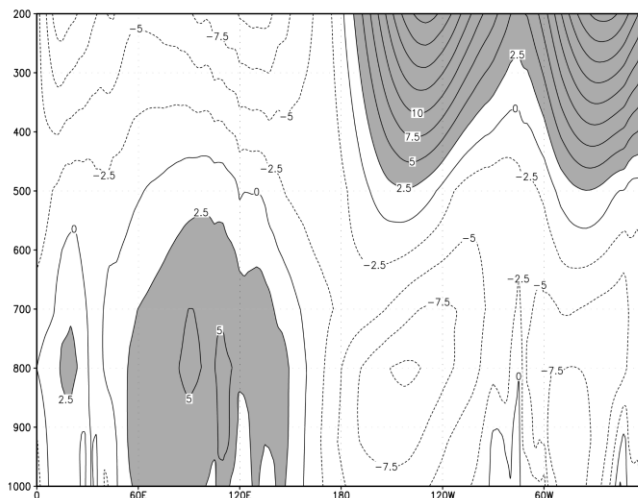


155

156

157 **Figure 3: Lagged-cross correlation between PC2 and the wind field at 200 hPa (vectors) and OLR anomalies (red and blue shading).**
158 **Contour interval: 0.2. The red and blue lines highlight the zone of antisymmetric OLR anomalies in the MRGW.**

159 The maximum amplitude of MRGWs at upper levels occurs over the westerly duct region at 200 hPa, but its amplitude
160 decreases over the Western Pacific, i.e., over a region with predominant easterly flow at upper tropospheric levels (Fig. 4). At
161 lower tropospheric levels, the westerly flow is observed over the western Pacific, where MRGWs have been documented
162 around 850hPa (Kiladis et al 2009). In this region, MRGWs may even lead to the formation of tropical cyclones (Dickinson
163 and Molinari, 2002; Zhou and Wang, 2007).



164

165

166

Figure 4: Vertical cross section of the climatological zonal wind (m.s-1) along the equator between December and February 1991-2020. Shading corresponds to regions of westerlies.

167

168

169

170

171

172

173

174

175

176

177

178

179

180

181

In the central eastern Pacific, MRGW activity is an important mechanism to modulate the lower tropospheric moisture field that results in tropical convection. Lagged cross correlations between PC1 and 700 hPa wind field and band-passed filtered anomalies of 700 hPa specific humidity show that in the central eastern Pacific MRGW modulate atmospheric moisture near the boundary layer. At lag -2 days, the sequence of clockwise and anticlockwise vortices corresponding to MRGWs along the equatorial Pacific begin to modulate the antisymmetric response in specific humidity over the eastern Pacific, around 100°W (Fig.5.a). At lag 0 days, the correspondence between the antisymmetric structure of anomalous atmospheric moisture off the equator and the divergent and convergent regions associated with the MRGW is more evident. The MRGW extends from the central Pacific into the Atlantic and the antisymmetric atmospheric moisture anomalies are observed in the corresponding divergent and convergent regions off the equator, between 5° and 10° in latitude and around 100°W. This equatorial disturbance exhibits a dominant zonal wavenumber 5 structure that extends into the Atlantic, in agreement with the westwards group velocity associated with MRGWs (Fig.5.b). At lag +2 days, the signal in specific humidity correlations moves westward, maintaining the antisymmetric structure off the equator and extending to the Atlantic Ocean (Fig. 5c). The antisymmetric structure in the specific humidity and divergence (around 140°W) – convergence anomalies extends westward with the characteristic phase velocity of MRGW, while their signal extends into the tropical Atlantic and northern South America in relation to their group velocity.



Specific Humidity and U;V (700 hPa) - Lag Correlation x PC 1

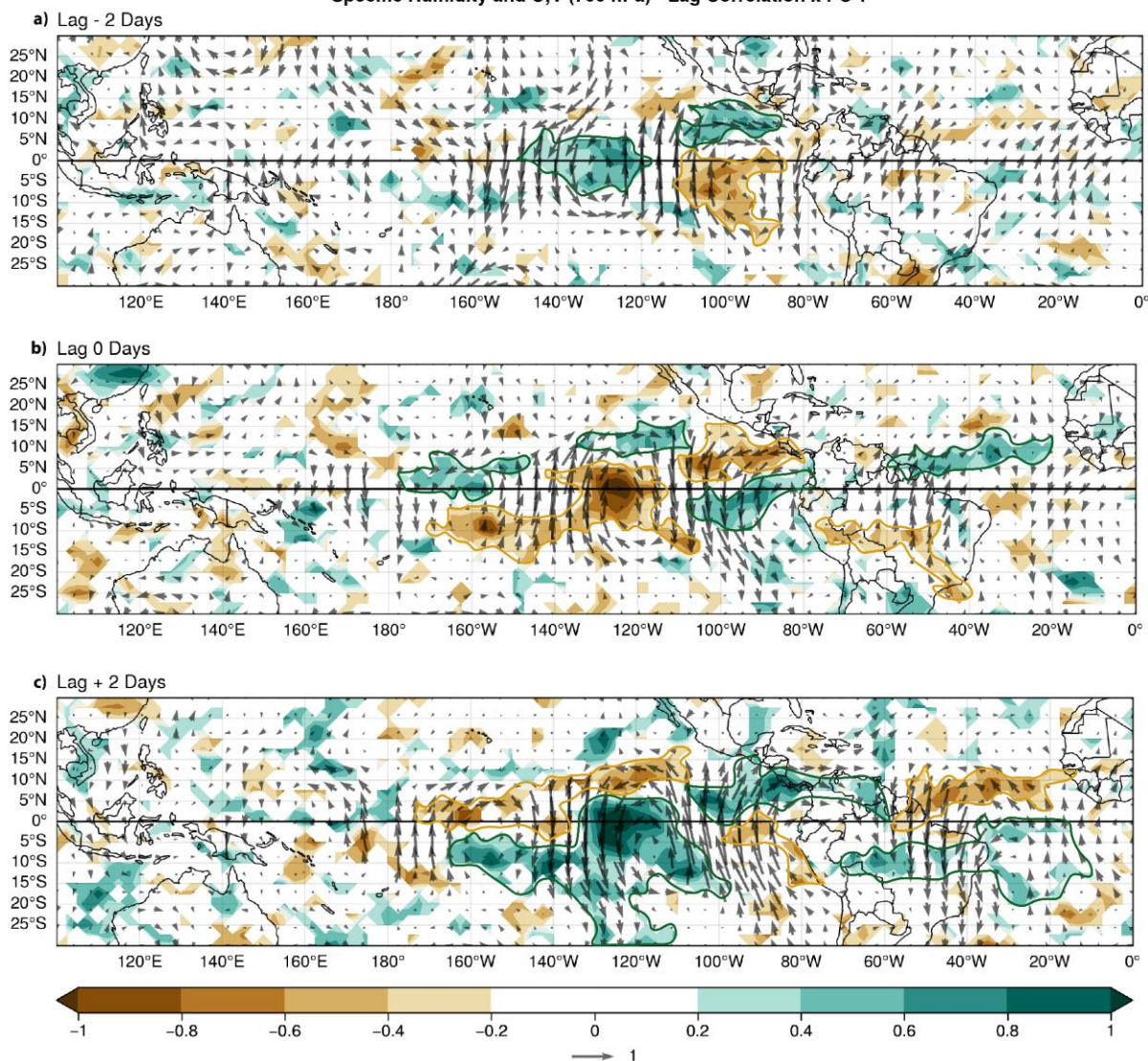


Figure 5: Lagged cross-correlation between the first principal component (PC1) of the 200 hPa meridional wind and the bandpass-filtered specific humidity (02–06 day periods; represented by shaded regions in green and brown), along with anomalies in the 700 hPa wind field (vectors), during the December–February period. Panels show results for: a) Lag -2 days, b) Lag 0 days, and c) Lag +2 days. Thick solid lines highlight regions of anomalous convective activity associated with the MRGW.

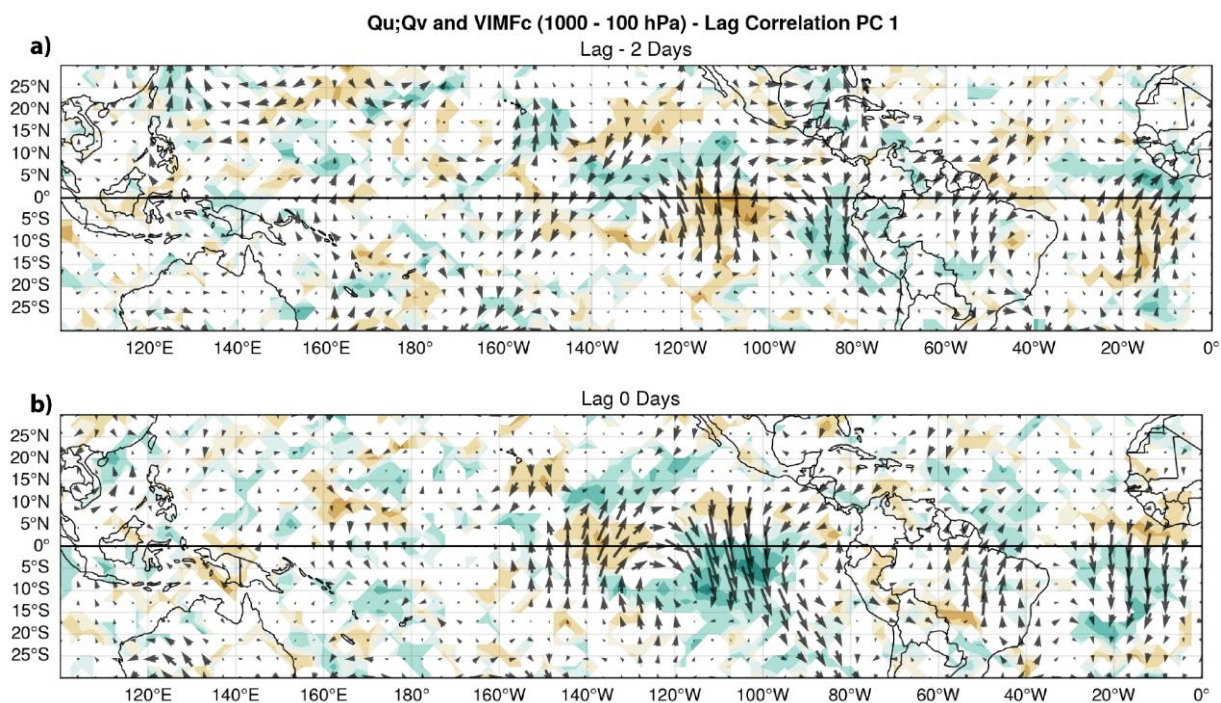
3.2 Vertically Integrated Moisture Flux in the tropics

The modulation of moisture by low level MRGW circulations is also diagnosed by examining the Vertically Integrated Moisture Flux (VIMF) and its convergence. As previously stated, VIMF is a measure of the amount of water vapor transported in the atmosphere and its convergence is used to determine zones of intense convective activity. The lagged correlations of PC1 and VIMF and its convergence show that a MRGW tends to create regions of moisture accumulation that result in tropical

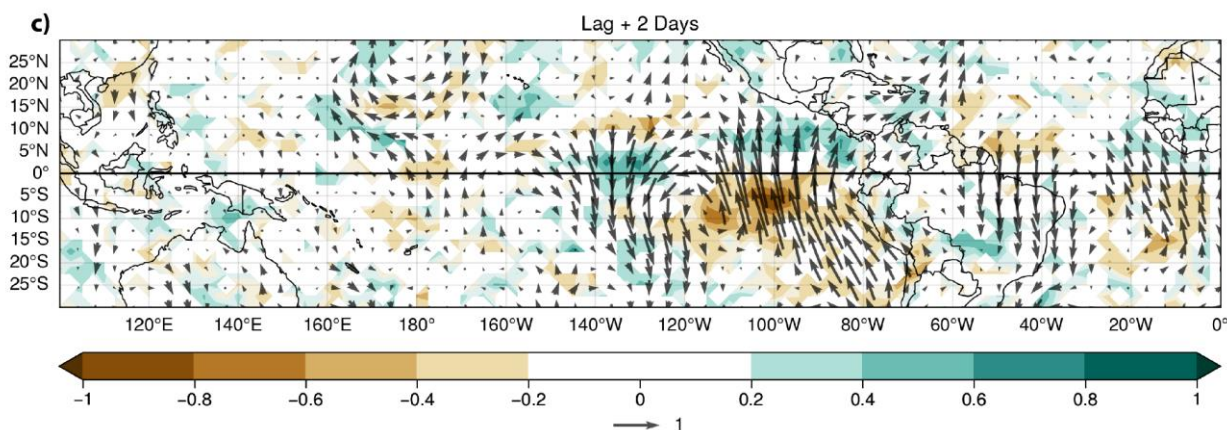


194 convective activity. By lag -2 days, the signals of a MRGW along the eastern equatorial Pacific and a midlatitude wave from
195 the northern subtropics along the westerly duct region show a tropical-midlatitude interaction (Fig.6.a). The positive and
196 negative vertical motion anomalies reflect in the regions of VIMF convergence and divergence in the midlatitude wave. In the
197 equatorial region, moisture convergence and divergence are located off the equator as expected in a MRGW. At lag 0 days,
198 VIMF and its convergence-divergence zones show the westward movement of the MRGW and the antisymmetric location of
199 the associated zones of moisture convergence and divergence (Fig. 6.b). The spatial structure of VIMF correlations
200 approximately match the one observed for the wind field anomalies at 700 hPa (see Fig.5.b) indicating that VIMF is capturing
201 the signal of MRGW at lower tropospheric levels. Such anomalous circulation modulates zones of specific humidity anomalies
202 off the equator in the central-eastern equatorial Pacific. By lag +2 days, the MRGW signal shows that moisture convergence
203 and divergence are asymmetrically distributed (Fig.6.c) contributing to increases and decreases of specific humidity, between
204 150°W and 70°W (see Fig. 5.c). The previous analysis shows that moisture is controlled by the MRGW at lower tropospheric
205 levels inducing zones of negative and positive convective activity anomalies. The quadrature between the phase of the MRGW
206 at upper and lower tropospheric levels serves to connect moisture convergence (divergence) at 700 hPa with divergence
207 (convergence) at 200 hPa, characteristics of deep tropical convective systems.

208



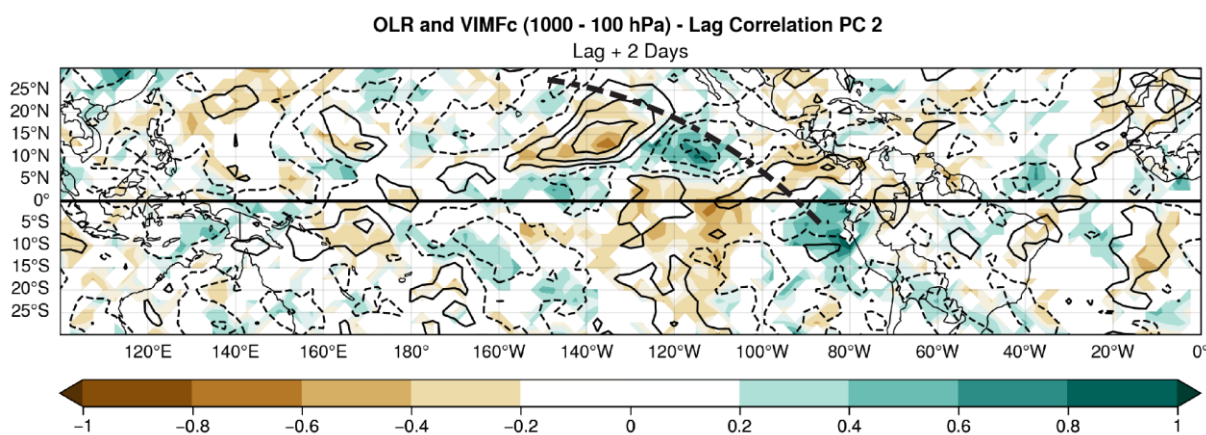
209



210

211 **Figure 6: Lagged-cross correlation between PC1 and VIMFc (vectors) and convergence (shades of green) and divergence (shades of**
 212 **brown) of VIMFc for the December – February months. a) Lag -2 days, b) Lag 0 days, and c) Lag +2 days.**

213 The relationship between VIMF convergence (VIMFc) and divergence, and OLR anomalies may be further examined by
 214 comparing the lag correlations between PC2 and VIMF convergence and OLR. For brevity, the relationship between VIMF
 215 and OLR correlations is shown only for lag +2 days. The signal of the midlatitude wave approaching the westerly duct region
 216 is observed as positive and negative correlations corresponding to VIMF convergence (divergence) and OLR negative
 217 (positive) anomalies. The signal extends into South America showing that not only it triggers a MRGW but also continues its
 218 interhemispheric propagation (Webster and Holton, 1982; Tomas and Webster, 1994; Li et al., 2015; Braga et al., 2022; Braga
 219 et al., 2024). Along the equatorial region the antisymmetric signals in correlation appear for VIMF convergence (divergence)
 220 and OLR anomalies extending from 150°W to 80°W.



221

222 **Figure 7: Lagged correlation between the second principal component (PC2) and outgoing longwave radiation (OLR) at lag +2 days,**
 223 **represented by solid (positive) and dashed (negative) lines. Shaded regions depict vertically integrated moisture flux convergence**
 224 **(VIMFc).**

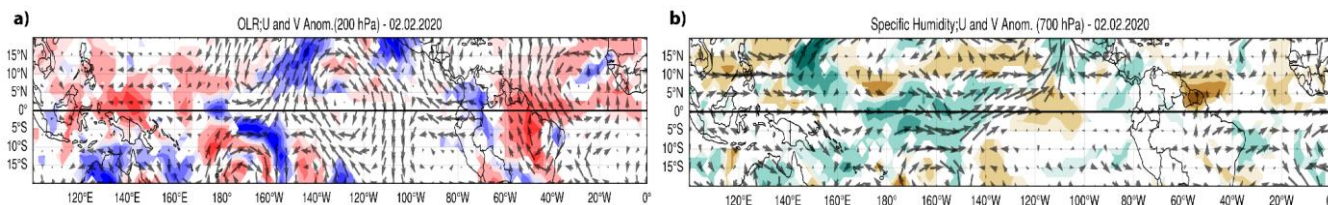


225 Over the eastern subtropical Pacific, in the region of tropical midlatitude interaction, positive signals of correlations for specific
226 humidity anomalies and OLR are observed extending into southern Mexico, that approximately correspond to the so-called
227 tropical plumes that at times correspond to precipitation events in this region (Knippertz, 2007; Fröhlich et al., 2013).

228 3.3 Case Study

229 An example of the presence of MRGWs in the daily atmospheric circulations is given in the wind field in upper and lower
230 tropospheric levels on February 2-6, 2020, identified as a large value of PC2. On February 2, 2020, a midlatitude wave over
231 the central-northeastern Pacific propagates into the tropics across the westerly duct region, coupled with the characteristic
232 circulation of a MRGW around 180°W. At 200 hPa (180°W-120°W) OLR positive and negative anomalies are observed in the
233 regions of ascending and descending motions associated with the midlatitude wave that propagates from the northern to the
234 southern hemisphere (Fig.8.a). The clockwise equatorial circulation at 200 hPa corresponds to part of the midlatitude wave
235 but it is also a characteristic of the equatorial MRGW. At lower tropospheric levels (700 hPa), there is only a slight signal of
236 this clockwise circulation, almost in phase with the upper tropospheric vortex. At 700 hPa, the midlatitude wave is hardly
237 present in the wind field around the subtropics but it shows negative and positive specific humidity anomalies in the
238 convergence and divergence regions around 20°N (Fig.8.b). By February 3, 2020, the midlatitude wave at 200 hPa extends to
239 the Pacific coast of South America with the corresponding positive and negative anomalies in OLR (Fig. 8c). At around 130°W,
240 a well-defined vortex corresponds to an equatorial clockwise circulation with antisymmetric OLR anomalies. At 700 hPa, a
241 clockwise circulation may also be identified at 140°W, with signals of a vortex that corresponds to the MRGW with positive
242 and negative specific humidity anomalies around (Fig.8.d). By February 4, 2020, the mid latitude wave in the Northern
243 Hemisphere subtropics remains, but it intensifies in the equatorial and the tropical Southern Hemisphere region (Fig.8.e). The
244 phase of the equatorial clockwise vortex around 130°W appears to remain locked. In the lower troposphere the clockwise
245 circulation in the equatorial region is better defined and the anti-symmetric structure in the surrounding specific humidity
246 anomalies, characteristic of the MRGW, begins to form between 180°W and 140°W (Fig.8.f). On February 5, 2020, the MRGW
247 began its westward movement with anti-symmetric OLR anomalies better defined on its westward side. The midlatitude wave
248 signal in the north-central Pacific weakens (Fig.8.g). At lower levels the clockwise circulation associated with the MRGW is
249 well defined over the equator and shows a westward displacement with the specific humidity anomalies anti-symmetrically
250 distributed around this circulation, in the moisture convergent and divergent regions (Fig.8.h). The structure of the MRGW at
251 700 hPa appears to be better defined as it approaches the westerly winds, west of the dateline.

252



253

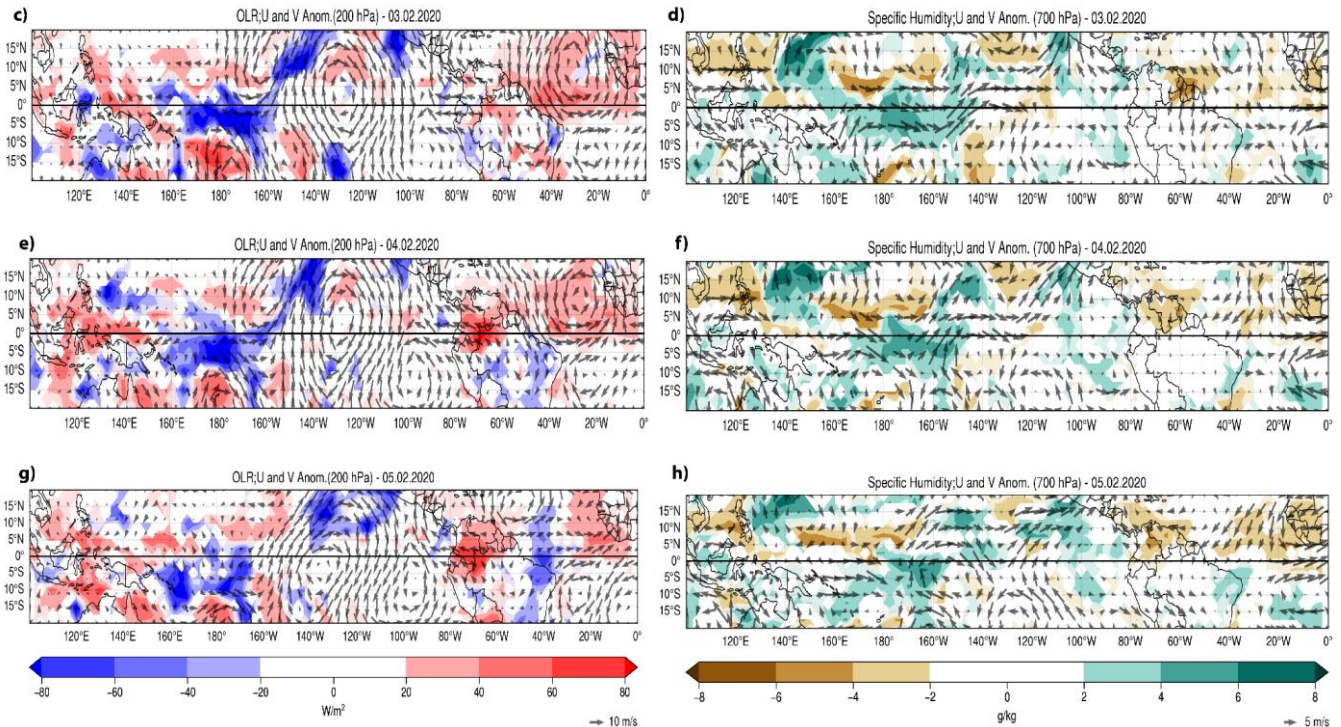
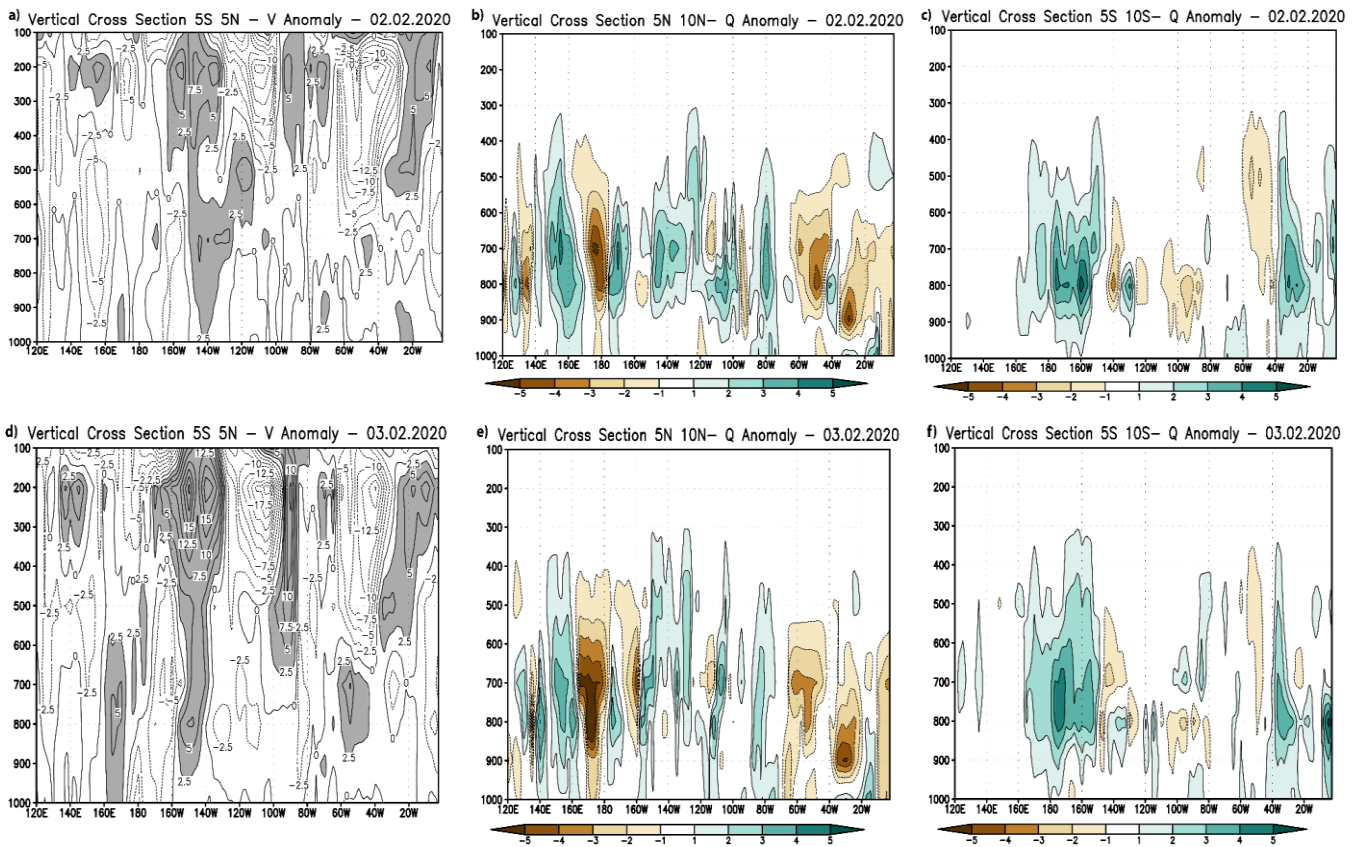


Figure 8: Anomalies in atmospheric conditions (200 hPa wind and OLR in the left column, 700 hPa wind and specific humidity in the right column) from February 2 to 5, 2020: (a) and (b) for February 2, (c) and (d) for February 3, (e) and (f) for February 4, and (g) and (h) for February 5.

As observed by Zhou and Wang (2007) in their case study of a MRGW, this equatorial wave is triggered at upper tropospheric levels and its signal propagates downward in the following days. The sequence of atmospheric circulations between 02-05 February 2020 shows that the equatorial wave circulations are well defined in the early days at 200 hPa, and its presence is better detected at later stages at 700 hPa. A vertical cross section of the meridional wind anomalies along the equator and specific humidity anomalies north and south of the equator (5°N-5°S) reflect the development of the vertical structure of the MRGW. The vertical cross section of the meridional wind anomalies between 5°S and 5°N (Fig.9.a) and specific humidity anomalies between 5°S and 10°S (Fig.9.b) and 5°N and 10°N (Fig.9.c), for February 2, 2020, shows that the signal of the MRGW in the wind field is present mainly at 200 hPa around 160°W-100°W, with magnitude of around 15 ms⁻¹, between 100 and 400 hPa. At this stage of development, the specific humidity anomalies do not appear to correspond to the moisture convergence and divergence induced by a MRGW. By February 3, 2020, the signal of the MRGW in the central eastern Pacific, at upper tropospheric levels, extends downward to around 700 hPa (Fig.9.d). Some indications of the induced effect of the lower tropospheric part of the MRGW show in the specific humidity, with positive-negative anomalies around 700 hPa, between 160°E and 140°W (Fig.9.e). South of the equator the sign of these anomalies tends to be the opposite to its northward counterpart, but still is not well defined (Fig.9.f). By February 4, 2020, the quadrature in the anomalies of the meridional component of the wind field shows and extends to lower tropospheric levels with an eastward tilt with height at around 150°W



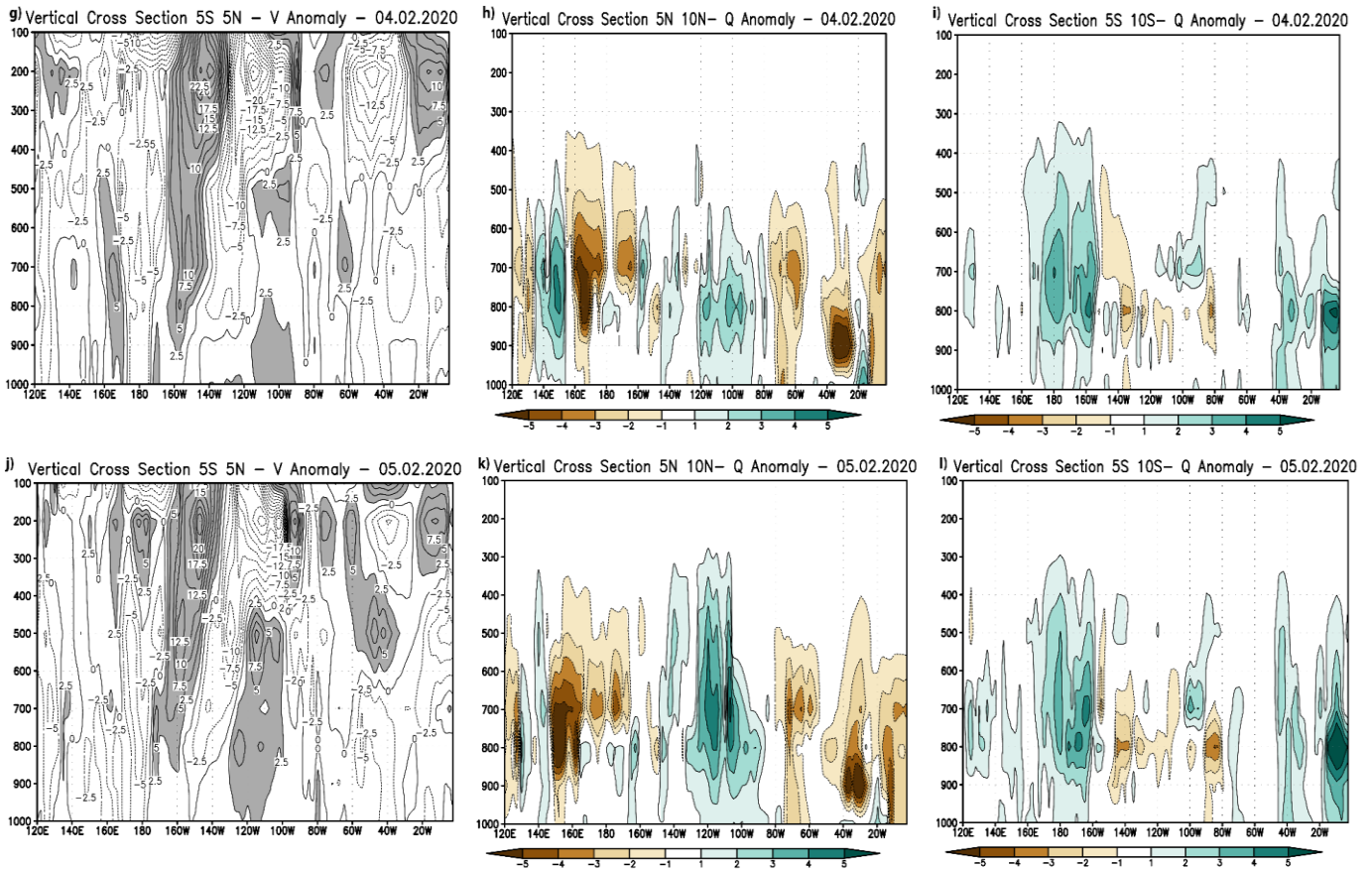
275 (Fig.9.g). The tilt with height approximately corresponds to a vertical wavelength of around 15 km, which approximately
276 agrees with early estimates by Yanai and Hayashi (1969). At around 700 hPa positive and negative anomalies appear induced
277 by moisture convergence and divergence associated with the MRGW (Fig.9.h.i). On February 5, 2020, the structure of the
278 MRGW in the troposphere exhibits the tilt with height associated with the vertical wavelength between 180°W and 120°W
279 (Fig.9.j). North and South of the equator antisymmetric anomalies in the specific humidity field are well defined in association
280 with the circulations induced by the MRGW (Fig.9.k.l). This case study suggests that the moisture anomalies in the lower
281 tropospheric levels tend to develop as the MRGW propagates downward from the upper tropospheric levels where it was
282 triggered by a midlatitude wave. Once MRGW is well developed, it modulates moisture convergence and develops as deep
283 convection thanks to the wind divergence in the upper troposphere.



284

285

286



287

288

289 **Figure 9:** Vertical cross-sections (longitude – height) (1000–100 hPa, between 5°S–5°N) for daily meridional wind anomalies (left
290 column) and daily specific humidity anomalies (central and right columns) from February 2 to 5, 2020: (a), (b), and (c) for February
291 2; (d), (e), and (f) for February 3; (g), (h), and (i) for February 4; and (j), (k), and (l) for February 5.

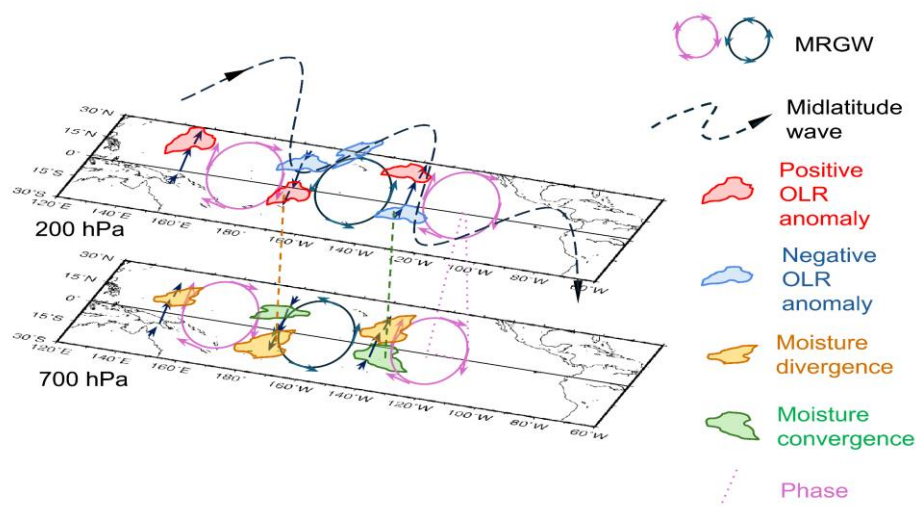
292 4. Summary and Conclusions

293 Upon the discovery of forced equatorial waves, numerous studies have proposed that they are forced either, by a midlatitude
294 wave propagating into the tropics, or by convective activity near the equatorial regions. Lateral forcing appears to be a
295 frequently accepted triggering mechanism for MRGW (Magaña and Yanai, 1995; Zhou and Wang, 2007; Shreya and Suhas,
296 2024). However, there is still some debate on the relationship between MRGW and the associated tropical convective activity.
297 Even more, the signals of MRGW in the upper and lower troposphere are often treated separately.

298 The present studies show a plausible explanation to coherently relate all these various elements considering midlatitude wave
299 forcing of equatorial circulation with the characteristics of a MRGW. As suggested by Au-Yeung and Tam (2018), the present
300 studies shows that the signal of the MRGW extends to the lower troposphere where it changes the atmospheric moisture field,
301 which in turn, results in antisymmetric anomalies in specific humidity off the equator, as those reported in other observational
302 analyses (eg. Kiladis et al., 2009). The phase difference (quadrature) between the upper tropospheric MRGW circulations



303 (wind convergence-divergence) and its lower tropospheric counterpart (moisture divergence-convergence) reinforce the
304 development of deep tropical convection that shows as positive and negative OLR anomalies (Fig.10). Therefore, a key element
305 to associate convective activity and atmospheric circulation in a MRGW is the eastward tilt with height in the troposphere that
306 results in a quadrature of the phase of the wave. From the top of the troposphere to the stratosphere the westward tilt with
307 height corresponds to the vertical structure of the MRGW (e.g Holton, 1979).



308
309 **Figure 10: Schematic of the vertical structure of a MRGW and the corresponding circulation anomalies in lower and upper**
310 **tropospheric levels along with moisture and convective activity signals in divergent and convergent regions of the wave.**

311 The development of MRGW constitutes a process that involves tropical midlatitude interactions that may be of relevance for
312 weather in the tropical region, where moisture convergence in the eastern tropical Pacific induced by MRGW constitute the
313 source of convective activity, even for tropical plumes observed over Mexico during the boreal winter season (Knippertz,
314 2007; Fröhlich et al., 2013). In addition, the propagation of the midlatitude wave into the Southern Hemisphere through the
315 westerly duct affects weather over South America (Braga et al., 2022).

316 Thanks to the improvement of atmospheric reanalysis, it is now possible to more accurately describe the characteristics of
317 equatorial waves in the troposphere and even in the stratosphere. A systematic identification of equatorial wave activity may
318 serve to better define the influence of these systems in weather in several tropical regions, for instance in the tropical Americas.
319 In summary, a key element of tropical weather in the eastern Pacific are MRGWs and consequently, a better understanding of
320 the processes of modulation of atmospheric moisture and convective activity may significantly improve weather forecasts in
321 the tropical and subtropical regions.

323 Author Declaration

324 **Funding information:** This work was supported by UNAM Postdoctoral Program (POSDOC), DGPA 13189. Victor Magaña.
325 was supported by the CONAHCYT Grant PCC-319779



326 **Conflicts of interest:** There is no conflict of interest.

327 **Ethics approval:** All authors have approved this manuscript.

328 **Consent to participate:** All authors have provided their consent to submit this manuscript to Weather and Climate Dynamics.

329 **Consent for publication:** All authors give permission to publish this manuscript.

330 **Data availability:** Publicly available datasets were analyzed in this study. This data can be found here:
331 <https://www.ecmwf.int/en/forecasts/dataset/ecmwf-reanalysis-v5>.

332 **Authors' contributions:** Hugo A. Braga analyzed the data, wrote the manuscript, and prepared the figures. Victor Magaña
333 contributed some parts and reviewed the manuscript together with the first author.

334 **Acknowledgements:** We would like to express our gratitude to the Departamento de Geografía Física at the Instituto de
335 Geografía, UNAM for their support. The technical assistance provided by Gustavo Vázquez is highly appreciated. We also
336 thank DGAPA-UNAM 13189 for the postdoctoral fellowship that made this project possible, as well as CONAHCYT Grant
337 PCC-319779.

338 **References**

339 Au-Yeung, A. Y. M., and C.-Y. Tam: Dispersion characteristics and circulation associated with boreal summer westward-
340 traveling mixed Rossby–gravity wave–like disturbances, *J. Atmos. Sci.*, 75(2), 513–533, [https://doi.org/10.1175/JAS-D-16-](https://doi.org/10.1175/JAS-D-16-0245.1)
341 0245.1, 2018.

342 Bennet, J.R., and J.A. Young: The influence of latitudinal with shear upon large-scale wave propagation into the tropics, *Mon.*
343 *Wea. Rev.*, 99, 201–214, https://doi.org/10.2151/jmsj1965.52.3_261,1971.

344 Braga, H. A., T. Ambrizzi, and N. M. J. Hall: Relationship between interhemispheric Rossby wave propagation and South
345 Atlantic Convergence Zone during La Niña years, *Int. J. Climatol.*, 13, <https://doi.org/10.1002/joc.7755>, 2022.

346 Braga, H.A., Ambrizzi, T., and Hall, N.M.J.: South Atlantic Convergence Zone as Rossby wave source, *Theor. Appl. Climatol.*,
347 155, 4231–4247, <https://doi.org/10.1007/s00704-024-04877-y>, 2024.

348 Dickinson, M., and J. Molinari: Mixed Rossby–Gravity Waves and Western Pacific Tropical Cyclogenesis. Part I: Synoptic
349 Evolution, *J. Atmos. Sci.*, 59, 2183–2196, [https://doi.org/10.1175/1520-0469\(2002\)059<2183>2.0.CO;2](https://doi.org/10.1175/1520-0469(2002)059<2183>2.0.CO;2), 2002.

350 Duchon, C. E.: Lanczos filtering in one and two dimensions, *J. Appl. Meteor. Climatol.*, 18(8), 1016–1022,
351 [https://doi.org/10.1175/1520-0450\(1979\)018<1016>2.0.CO;2](https://doi.org/10.1175/1520-0450(1979)018<1016>2.0.CO;2), 1979.

352 Fasullo, J., and P. J. Webster: A hydrological definition of Indian monsoon onset and withdrawal, *J. Clim.*, 16(19), 3200–3211,
353 [https://doi.org/10.1175/1520-0442\(2003\)016<3200>2.0.CO;2](https://doi.org/10.1175/1520-0442(2003)016<3200>2.0.CO;2), 2003.

354 Fröhlich, L., P. Knippertz, A. H. Fink, and E. Hohberger: An objective climatology of tropical plumes, *J. Clim.*, 26, 5044–
355 5060, <https://doi.org/10.1175/JCLI-D-12-00351.1>, 2013.

356 Hayashi, Y.: A theory of large-scale equatorial waves generated by condensation heat and accelerating, *J. Meteor. Soc. Jpn.*
357 *Ser. II*, 48(2), 140–160, https://doi.org/10.2151/jmsj1965.48.2_140, 1970.



- 358 Hayashi, Y.: Interpretations of space-time spectral energy equations, *J. Atmos. Sci.*, 39(3), 685–688,
359 [https://doi.org/10.1175/1520-0469\(1982\)039<0685>2.0.CO;2](https://doi.org/10.1175/1520-0469(1982)039<0685>2.0.CO;2), 1982.
- 360 Hayashi, Y., and D. G. Golder: The generation of equatorial transient planetary waves: Control experiments with a GFDL
361 general circulation model, *J. Atmos. Sci.*, 35(11), 2068–2082, [https://doi.org/10.1175/1520-0469\(1978\)035<2068>2.0.CO;2](https://doi.org/10.1175/1520-0469(1978)035<2068>2.0.CO;2),
362 1978.
- 363 Hess, P., H. Hendon, and D. S. Battisti: The relationship between mixed Rossby gravity waves and convection in a general
364 circulation model, *J. Meteor. Soc. Jpn.*, 71, 321–338, 1993.
- 365 Hersbach, H., and Coauthors: The ERA5 global reanalysis, *Q. J. R. Meteorol. Soc.*, 146(730), 1999–2049,
366 <https://doi.org/10.1002/qj.3803>, 2020.
- 367 Holton, J. R.: Waves in the equatorial stratosphere generated by tropospheric heat sources, *J. Atmos. Sci.*, 29(2), 368–375,
368 [https://doi.org/10.1175/1520-0469\(1972\)029<0368>2.0.CO;2](https://doi.org/10.1175/1520-0469(1972)029<0368>2.0.CO;2), 1972.
- 369 Holton, J.R.: *An Introduction to Dynamic Meteorology*, Academic Press, New York, 391 pp., 1979.
- 370 Kiladis, G. N., M. C. Wheeler, P. T. Haertel, K. H. Straub, and P. E. Roundy: Convectively coupled equatorial waves, *Rev.*
371 *Geophys.*, 47(2), <https://doi.org/10.1029/2008RG000266>, 2009.
- 372 Knippertz, P.: Tropical–extratropical interactions related to upper-level troughs at low latitudes, *Dyn. Atmos. Oceans*, 43(1–
373 2), 36–62, <https://doi.org/10.1016/j.dynatmoce.2006.06.003>, 2007.
- 374 Li, Y., J. Li, F. F. Jin, and S. Zhao: Interhemispheric propagation of stationary Rossby waves in a horizontally nonuniform
375 background flow, *J. Atmos. Sci.*, 72(8), 3233–3256, <https://doi.org/10.1175/JAS-D-14-0239.1>, 2015.
- 376 Li, Y., J. Feng, J. Li, and A. Hu: Equatorial windows and barriers for stationary Rossby wave propagation, *J. Clim.*, 32, 6117–
377 6135, <https://doi.org/10.1175/JCLI-D-18-0722.1>, 2019.
- 378 Liebmann, B., and C. A. Smith: Description of a complete (interpolated) outgoing longwave radiation dataset, *Bull. Am.*
379 *Meteor. Soc.*, 77(6), 1275–1277, <https://doi.org/10.2307/26233278>, 1996.
- 380 Magaña, V., and M. Yanai: Tropical-midlatitude interaction on the time scale of 30 to 60 days during the Northern summer of
381 1979, *J. Clim.*, 4, 180–201, [https://doi.org/10.1175/1520-0442\(1991\)004<0180>2.0.CO;2](https://doi.org/10.1175/1520-0442(1991)004<0180>2.0.CO;2), 1991.
- 382 Magaña, V., and M. Yanai: Mixed Rossby–gravity waves triggered by lateral forcing, *J. Atmos. Sci.*, 52(9), 1473–1486,
383 [https://doi.org/10.1175/1520-0469\(1995\)052<1473>2.0.CO;2](https://doi.org/10.1175/1520-0469(1995)052<1473>2.0.CO;2), 1995.
- 384 Mak, M.: Laterally driven stochastic motions in the tropics, *J. Atmos. Sci.*, 26, 41–64, [https://doi.org/10.1175/1520-0469\(1969\)026<0041>2.0.CO;2](https://doi.org/10.1175/1520-0469(1969)026<0041>2.0.CO;2), 1969.
- 386 Maruyama, T.: Large-scale disturbances in the equatorial lower stratosphere, *J. Meteor. Soc. Jpn. Ser. II*, 45(5), 391–408,
387 https://doi.org/10.2151/jmsj1965.45.5_391, 1967.
- 388 Matsuno, T.: Quasi-geostrophic motions in the equatorial area, *J. Meteor. Soc. Jpn. Ser. II*, 44(1), 25–43,
389 https://doi.org/10.2151/jmsj1965.44.1_25, 1966.
- 390 Nitta, T.: Statistical study of tropospheric wave disturbances in the tropical Pacific region, *J. Meteor. Soc. Jpn. Ser. II*, 48(1),
391 47–60, https://doi.org/10.2151/jmsj1965.48.1_47, 1970.



- 392 Pazos, M., V. Magaña, and E. Herrera: Easterly wave activity in the Intra-Americas Seas region analyzed with vertically
393 integrated moisture fluxes, *Front. Earth Sci.*, 11, 1223939, <https://doi.org/10.3389/feart.2023.1223939>, 2023.
- 394 Shreya, K., and E. Suhas: A survey of westward-propagating mixed Rossby–Gravity waves and quantification of their
395 association with extratropical disturbances, *Q. J. R. Meteorol. Soc.*, 1–19, <https://doi.org/10.1002/qj.4668>, 2024.
- 396 Takayabu, N. Y., and T. Nitta: 3–5 day-period disturbances coupled with convection over the tropical Pacific Ocean, *J. Meteor.*
397 *Soc. Jpn.*, 71, 221–245, https://doi.org/10.2151/jmsj1965.71.2_221, 1993.
- 398 Tomas, R. A., and P. J. Webster: Horizontal and vertical structure of cross-equatorial wave propagation, *J. Atmos. Sci.*, 51(11),
399 1417–1430, [https://doi.org/10.1175/1520-0469\(1994\)051<1417>2.0.CO;2](https://doi.org/10.1175/1520-0469(1994)051<1417>2.0.CO;2), 1994.
- 400 Webster, P. J., and J. R. Holton: Cross-equatorial response to middle-latitude forcing in a zonally varying basic state, *J. Atmos.*
401 *Sci.*, 39(4), 722–733, [https://doi.org/10.1175/1520-0469\(1982\)039<0722>2.0.CO;2](https://doi.org/10.1175/1520-0469(1982)039<0722>2.0.CO;2), 1982.
- 402 Wheeler, M., and G. N. Kiladis: Convectively coupled equatorial waves: Analysis of clouds and temperature in the
403 wavenumber–frequency domain, *J. Atmos. Sci.*, 56, 374–399, [https://doi.org/10.1175/1520-0469\(1999\)056<0374>2.0.CO;2](https://doi.org/10.1175/1520-0469(1999)056<0374>2.0.CO;2),
404 1999.
- 405 Yanai, M., and Y. Hayashi: Large-scale equatorial waves penetrating from the upper troposphere into the lower stratosphere,
406 *J. Meteor. Soc. Jpn. Ser. II*, 47(3), 167–182, https://doi.org/10.2151/jmsj1965.47.3_167, 1969.
- 407 Yanai, M., and T. Maruyama: Stratospheric wave disturbances propagating over the equatorial Pacific, *J. Meteor. Soc. Jpn.*
408 *Ser. II*, 44(5), 291–294, https://doi.org/10.2151/jmsj1965.44.5_291, 1966.
- 409 Yanai, M., and M. Murakami: A further study of tropical wave disturbances by the use of spectrum analysis, *J. Meteor. Soc.*
410 *Jpn. Ser. II*, 48(3), 185–197, https://doi.org/10.2151/jmsj1965.48.3_185, 1970a.
- 411 Yanai, M., and M. Murakami: Spectrum analysis of symmetric and antisymmetric equatorial waves, *J. Meteor. Soc. Jpn. Ser.*
412 *II*, 48(4), 331–347, <https://doi.org/10.2151/jmsj1965.48.4331>, 1970b.
- 413 Yanai, M., and M. Lu: Equatorially trapped waves at the 200 mb level and their association with meridional convergence of
414 wave energy flux, *J. Atmos. Sci.*, 40, 2785–2803, [https://doi.org/10.1175/1520-0469\(1983\)040<2785>2.0.CO;2](https://doi.org/10.1175/1520-0469(1983)040<2785>2.0.CO;2), 1983.
- 415 Yang, G., B. Hoskins, and J. Slingo: Convectively coupled equatorial waves: A new methodology for identifying wave
416 structures in observational data, *J. Atmos. Sci.*, 60, 1637–1654, [https://doi.org/10.1175/1520-0469\(2003\)060<1637>2.0.CO;2](https://doi.org/10.1175/1520-0469(2003)060<1637>2.0.CO;2),
417 2003.
- 418 Zhou, X., and B. Wang: Transition from an eastern Pacific upper-level mixed Rossby-gravity wave to a western Pacific tropical
419 cyclone, *Geophys. Res. Lett.*, 34, L24801, <https://doi.org/10.1029/2007GL031831>, 2007.
- 420 Zhang, C., and P. J. Webster: Laterally forced equatorial perturbations in a linear model. Part I: Stationary transient forcing, *J.*
421 *Atmos. Sci.*, 49, 585–607, [https://doi.org/10.1175/1520-0469\(1992\)049<0585>2.0.CO;2](https://doi.org/10.1175/1520-0469(1992)049<0585>2.0.CO;2), 1992.